ELSEVIER

Coastal Engineering 42 (2001) 359–373

Coastal Engineering
An International Journal for Coastal, Harbour and Offshore Engineers

www.elsevier.com/locate/coastaleng

Simulation of wave breaking effects in two-dimensional elliptic harbor wave models

Liuzhi Zhao [a], Vijay Panchang [b,*], W. Chen [a], Z. Demirbilek [c], N. Chhabbra [d]

[a] *Civil Engineering Department, University of Maine, Orono, ME 04469-5706, USA*
[b] *School of Marine Sciences, University of Maine, Orono, ME 04469-5706, USA*
[c] *US Army Engineer Research and Development Center, Coastal and Hydraulics Laboratory, Vicksburg, MS 39180, USA*
[d] *GE Power Systems, 1 River Road, Schenectady, NY 12345, USA*

Received 8 February 2000; accepted 15 December 2000

Abstract

A technique is developed for including the effects of dissipation due to wave breaking in two-dimensional elliptic models based on the mild-slope wave equation. This involves exploration of convergence properties pertaining to iteration due to presence of the nonlinear wave breaking parameter in the governing equations as well as new boundary conditions that include wave-breaking effects. Five wave-breaking formulations are examined in conjunction with the resulting model, which is applied to tests involving a sloping beach, a bar-trough bottom configuration, shore-connected and shore-parallel breakwaters on a sloping beach, and two real-world cases. Model results show that three of the formulations, when used within the context of the modeling scheme presented here, provide excellent results compared to data.

Keywords: Wave; Model; Mild-slope equation; Breaking; Elliptic model

1. Introduction

Surface gravity waves in harbors are usually modelled using the two-dimensional mild-slope wave equation. This elliptic equation is intended to reproduce simultaneously the effects of refraction, diffraction, and reflection (due to structures as well as bathymetric variations) in domains of arbitrary shape for the entire spectrum of practical wave conditions. Several computational models have been developed utilizing this equation (e.g. Mei, 1983; Tsay and Liu, 1983; Chen and Houston, 1987; Kostense et al., 1986; Mattioli, 1996; Demirbilek and Panchang, 1998) and many have made their way into engineering practice (see review of contemporary models in Panchang et al., 1999). A major limitation in most of these models, though, is that they do not account for the effects of wave breaking. As such, the models frequently yield inordinately high values of wave heights, especially in shallow areas. In this paper, we discuss the inclusion of wave breaking in a two-dimensional mild-slope elliptic wave model.

* Corresponding author. U.S. Department of Commerce, National Oceanic and Atmospheric Administration, NSGO/NOAA, 1315 East-West Highway, Silver Spring, MD 20910, USA.
E-mail address: vijay.panchang@noaa.gov (V. Panchang).

0378-3839/01/$ - see front matter
PII: S0378-3839(00)00069-7

Several investigators (e.g. Booij, 1981; de Girolamo et al., 1988; Massel, 1992; Isobe, 1999; Chawla et al., 1998) have proposed that breaking can be introduced in the mild-slope equation in the form of a parameterized dissipation term as follows:

$$\nabla \cdot \left(CC_g \nabla \phi\right) + \left(CC_g k^2 + iC_g \sigma\gamma\right)\phi = 0 \qquad (1)$$

where $\phi(x,y)$ = complex surface elevation function $(=\phi_1 + i\phi_2)$; $i=\sqrt{-1}$; σ = wave frequency under consideration; $C(x,y)$ = phase velocity $= \sigma/k$; $C_g(x,y)$ = group velocity $= \partial\sigma/\partial k$; γ = wave breaking factor; $k(x,y)$ = wavenumber $(=2\pi/L)$, related to the local depth $d(x,y)$ through the dispersion relation:

$$\sigma^2 = gk\tanh(kd) \qquad (2)$$

The wave height H can be obtained from complex surface elevation function ϕ as follows:

$$H = \frac{2\sigma}{g}\sqrt{\left(\phi_1^2 + \phi_2^2\right)} \qquad (3)$$

The wave breaking factor γ contained in the last term of Eq. (1) can be parameterized in several ways (discussed later). However, all parameterizations are a function of the wave height and render the model nonlinear. The nonlinearity can be handled in a fairly straight-forward manner if only approximate paraxial solutions to Eq. (1) are sought, typically via the "parabolic equation method" (Chawla et al., 1998) or other comparable approximate models (Ebersole, 1985). In these methods, a solution is obtained by progressing from one computational row to the next in the shoreward direction. The solution along the previous row, therefore, can be used to estimate γ. In domains of complex shape involving unlimited angular scattering, these paraxial approximations are inadequate and the full elliptic equation must be solved. Solutions are then obtained simultaneously over all grid points in the domain, and no "prior row" values are available to estimate γ. Further, the inclusion of breaking invalidates the traditional open boundary conditions in which components of ϕ are generally based on non-breaking plane-wave representations (e.g. Mei, 1983; Xu et al., 1996).

In this paper, we develop a technique for incorporating wave breaking effects in a two-dimensional elliptic harbor wave model and explore the behavior of solution when breaking is included. The layout of the paper is as follows. The governing equations, including the development of an approximate but reasonably realistic formulation of open boundary conditions, are described in Section 2. Section 3 describes strategies for obtaining numerical solutions for the nonlinear problem; since the overall solution can be extremely time-intensive, efforts to obtain greater efficiency are also explored. Various breaking wave parameterizations that are suitable for this problem are presented in Section 4; these are used with the model developed to perform validation and field simulations in Section 5. Section 6 provides a summary and concluding remarks.

2. Model formulation

Fig. 1 shows a typical harbor wave model domain that may include arbitrarily shaped coastlines, islands, structures, and variable bathymetry. The semi-circle separates the computational domain Ω from the exterior sea. Within Ω the coastal boundary condition is

$$\frac{\partial\phi}{\partial n} = \alpha\phi \qquad (4)$$

where n is the outward normal to the boundary and α is related to a user-specified boundary reflection coefficient K_r as follows:

$$\alpha = ik\frac{1-K_r}{1+K_r} \qquad (5)$$

In the exterior domain Ω' the potential ϕ is comprised of three components:

$$\phi = \phi_i + \phi_r + \phi_s \qquad (6)$$

where ϕ_i = the incident wave that must be specified to force the model, ϕ_r = a reflected wave that would exist in the absence of the harbor, and ϕ_s = a scattered wave that emanates as a consequence of the harbor. With appropriate descriptions for these components, a boundary condition can be developed along the semicircle.

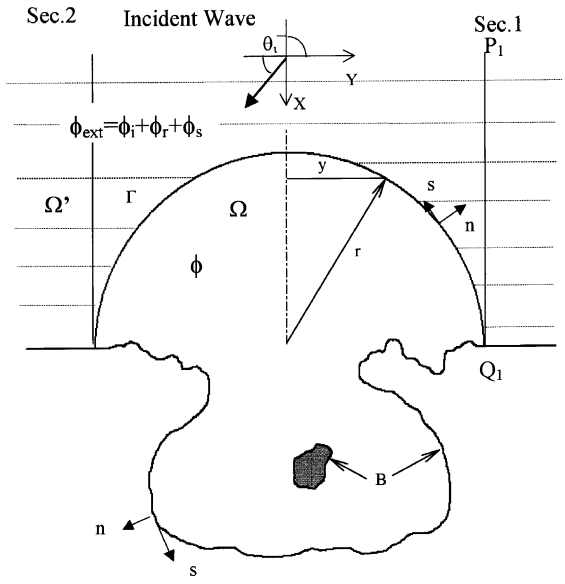

Fig. 1. Harbor wave model domain; definition sketch.

We will first discuss formulation of ϕ_i and ϕ_r. In most elliptic models (e.g. Xu et al., 1996; Tsay and Liu, 1983; Kostense et al., 1986; Chen, 1986), these are described as plane waves:

$$\phi_i = A_i \exp\left(ikr\cos(\theta - \theta_i)\right) \tag{7}$$

$$\phi_r = K_{re} A_i \exp\left(ikr\cos(\theta + \theta_i)\right) \tag{8}$$

where A_i and θ_i represent the incident wave amplitude and direction, (r, θ) denotes the location of a point in polar coordinates, and K_{re} represents the reflection coefficient for the exterior coastline. Eqs. (7) and (8) implicitly assume that the exterior depth is constant; most real domains, however, show generally increasing depths in the offshore direction. Further, the plane wave formulations do not contain the effects of breaking, and, when used in conjunction with the governing equation (Eq. (1)) in the interior that contains breaking, lead to a discontinuity along the open boundary as a result of incorrect forcing. To overcome this limitation, we assume that the depths in the exterior vary only in the x-direction along section 1 shown in Fig. 1. If natural variations do not permit the representation of the exterior depths by only one section, we may, if necessary, construct a second one-dimensional section, shown as section 2 in Fig. 1.

For sections 1 and 2 with varying depths, it is not possible to decouple ϕ_i and ϕ_r. However, they may be combined to form

$$\phi_0 = \phi_i + \phi_r \tag{9}$$

Since the depths along these sections vary in one direction only, ϕ_0 may be obtained by the solution of the one-dimensional version of Eq. (1). This may be obtained by describing the incident and reflected waves, at any point along section 1, as follows:

$$\phi_i = A(x)\exp(\int ik\cos\theta\, dx)\exp(iyk\sin\theta) \tag{10}$$

$$\phi_r = B(x)\exp(\int -ik\cos\theta dx)\exp(iyk\sin\theta) \tag{11}$$

Since $k\sin\theta$ is constant for one-dimensional geometry, ϕ_{01} for section 1 may be written as

$$\phi_{01} = \psi(x)\exp(iky\sin\theta) \tag{12}$$

which may be substituted into Eq. (1) to yield

$$\frac{d}{dx}\left(CC_g\frac{d\psi}{dx}\right) + kCC_g\left(k\cos^2\theta + i\gamma\right)\psi = 0 \tag{13}$$

Eq. (13), which constitutes a generalization of the one-dimensional linear shallow-water equation derived by Schaffer and Jonsson (1992), is an elliptic ordinary differential equation requiring two boundary conditions. Assuming that section 1 extends out to a region of constant depth (or deep water), a condition at P_1 may be obtained by combining a specified incident wave

$$\phi_i(P_1) = A_i\exp(ikx\cos\theta_i + iky\sin\theta_i) \tag{14}$$

(where A_i = a given input wave amplitude) and an unknown reflected wave:

$$\phi_r(P_1) = B\exp(-ikx\cos\theta_i + iky\sin\theta_i) \tag{15}$$

Without loss of generality, the point P_1 may be located at $x = 0$, which allows elimination of B to yield

$$\frac{\partial\psi}{\partial x} = ik\cos\theta_i(2A_i - \psi) \tag{16}$$

At the coastal boundary point Q_1, a partial reflection boundary condition may be used:

$$\frac{\partial \psi}{\partial x} = \frac{i\sqrt{k^2 - k^2 \sin^2\theta}\,(1 - K_r)}{1 + K_r}\psi \qquad (17)$$

where K_r is the reflection coefficient for the exterior coastline (i.e. near Q_1) (note that Eq. (17) is slightly more sophisticated than Eqs. (4) and (5) and follows Isaacson and Qu, 1990).

The solution of Eq. (13) using boundary conditions (16) and (17) along with Eq. (12) produces ϕ_0 along section 1. Similar equations may be used for section 2; note that if the bathymetry is strictly one-dimensional (i.e. if sections 1 and 2 are identical)

$$\phi_{01} = \phi_{02}\exp(ikl\sin\theta) \qquad (18)$$

where l is the alongshore separation between sections 1 and 2. The desired ϕ_0 along the semicircle may be obtained by laterally translating ϕ_{01} and ϕ_{02} via interpolation between sections 1 and 2 (described later), or if sections 1 and 2 are identical, through equations similar to Eq. (18).

The remainder of the exterior wavefield consists of the scattered wavefield ϕ_s that must radiate out to infinity with decreasing amplitude and may be approximately described (following Panchang et al. 2000; Behrendt, 1985) by:

$$\frac{\partial \phi_s}{\partial n} = \left(ik - \frac{1}{2r}\right)\phi_s \quad \text{along } \Gamma \qquad (19)$$

A boundary condition for ϕ along the semicircle Γ may be obtained by using the continuity of the potential (Eqs. (6) and (9)) and its derivative:

$$\frac{\partial \phi}{\partial n} = \frac{\partial \phi_0}{\partial n} + \left(ik - \frac{1}{2r}\right)(\phi - \phi_0) \qquad (20)$$

To summarize, the solution of Eq. (13) provides ϕ_0 along the one-dimensional sections. These values can be translated laterally and substituted into Eq. (20) to obtain the open boundary condition for the two-dimensional Eq. (1), which is solved in the model domain Ω, using, in addition, the coastal boundary condition given by Eq. (4).

3. Numerical solution

A digitized bathymetry file is used to obtain the depths $d(x)$ along section 1. These depths are interpolated onto uniformly spaced nodes and the wave properties C, C_g, and k are calculated. Eq. (13) is solved by finite-differences using boundary conditions (16) and (17). Since the wave breaking parameter is a function of the wave height (according to parameterizations described in Section 4) and is unknown a priori, Eq. (13) must be solved by iteration. For the first iteration, γ is set equal to 0 (i.e. non-breaking solutions are obtained). The resulting wave heights are used to estimate γ and Eq. (13) is solved again. The process is repeated until the solutions converge. ϕ_0 values along the nodes on section 1 are calculated using Eq. (12). This procedure is repeated for section 2 to obtain ϕ_{02}.

In the model interior Ω, the governing equation is solved via the finite element method. ϕ_0 values along the nodes on the semicircle are obtained by lateral translation of ϕ_{01} and ϕ_{02} as follows:

$$\phi_0 = (1 - w)\,\phi_{01}\exp(-ik(r - y)\sin\theta) + w\phi_{02}\exp(ik(r + y)\sin\theta) \qquad (21)$$

where, by setting $y = 0$ at the center of semicircle, the interpolation function $w = (r - y)/2r$, r is the radius of the semicircle, y is the lateral coordinate of the open boundary node relative to the origin of semicircle (Fig. 1). These ϕ_0 values contribute to the open boundary condition (20).

We used the Surface Water Modelling System (SMS), a graphical interface described by Zundell et al. (1998), to construct a triangular finite-element grid network in Ω. This package allows the convenient generation of wavelength-dependent grids and specification of the desired reflection coefficients on various segments of the solid boundary. Eq. (1) with boundary conditions (4) and (20) is solved via the Galerkin technique (Demirbilek and Panchang, 1998). Since a resolution of about 10 grids per local wavelength is generally needed for accurate solutions, an extremely large system of linear equations results. Iterative techniques based on the conjugate gradient methods described by Panchang et al. (1991) and Li (1994), which are guaranteed to converge,

were used to solve the linear equations. The solution was assumed to have converged when the following L2 norm was met:

$$\frac{\sum_{i=1}^{N}\left(\sum_{j=1}^{N}\mathbf{K}_{ij}\phi_j - \boldsymbol{F}_i\right)^2}{\sum_{i=1}^{N}|\phi_i|^2} < \varepsilon \qquad (22)$$

where $\mathbf{K}$ and $\boldsymbol{F}$ refer to the stiffness matrix and load vector, respectively, and ε is a specified tolerance (typically 10^{-10}). In general, the number of iterations is of the order of the number of nodes (typically of the order of 200,000). More recently, Oliveira and Anastasiou (1998) explored the use of the Generalized Minimum Residual method and the Stabilized Biconjugate Gradient method for greater efficiency with finite-difference models based on the linear version of Eq. (1). In our finite-element work, however, the GMRES method of Oliveira and Anastasiou (1998) failed to converge (as independently confirmed by Bogle (1999, personal communication)) whereas their latter method yielded erratic efficiency.

Significant improvements in speed were obtained by using two-level code parallelization for operation on high performance parallel computing platforms such as the SGI/Cray Origin2000 (O2K). For spectral simulations without interfrequency exchange, the solution of Eq. (1) for each monochromatic component leads to an independent system of linear equations. These equations are solved using distributed clusters of shared-memory multiprocessors (SMPs), which have to communicate and share the workload, e.g. via a Message Passing Interface, MPI. Individual wave components are distributed to multiple processors via MPI and load-balanced through the Manager–Worker model (Foster, 1997; Bova et al. 2000). At the second level, matrix operations are parallelized, since most of the CPU-time for each wave component is utilized in the solution of the linear system of equations. For conjugate gradient solvers, 90% of the CPU time is spent on matrix–vector products and inner product kernels. Therefore, OpenMP (OARB, 1997) was used to parallelize the kernels. Thus, the two-level parallelization used OpenMP to accelerate the solution for each component and MPI to simultaneously obtain solutions to multiple incident wave components. This led to a reduction in run times by a factor of about 200 for large, real-world applications. More details regarding parallelization schemes for harbor wave models may be found in Bova et al. (2000).

4. Wave breaking criteria and their implementation

In this paper, the effect of incorporating five wave breaking models into the simulation strategy described above was examined. The breaking models are based on the formulations of Battjes and Janssen (1978), Dally et al. (1985), Massel (1992), Chawla et al. (1998), and Isobe (1999) (the relevant formulas for γ are presented in Sections 4.1–4.5). Some of these parameterizations have been extensively validated against field data (e.g. Larson, 1995; Kamphuis, 1994). It is noted, however, that some of these parameterizations rely on spectral wave heights. Since the spectral conditions used while developing them were narrow-peaked, the monochromatic wave height is used in the parameterizations (as in De Girolamo et al., 1988) for monochromatic applications described here. However, the significant wave height (SWH) is used in spectral simulations (e.g. the last application described in Section 5). Eqs. (1) and (13) may be solved by iteration by estimating the nonlinear γ on the basis of the previous solution. The overall problem was assumed to have been solved when the maximum difference, δ, at any grid point between two successive nonlinear solutions reaches 10^{-3} or less. Further, the maximum number of non-linear iterations was set to 15 in the event of non-convergence or slow convergence.

To explore the behavior of the solution of this highly nonlinear problem and to design modifications as needed when the various breaking criteria are used with Eq. (1), the hydraulic model study of Battjes and Janssen (1978) describing wave propagation up a sloping beach was used as a benchmark. The model geometry is shown in Fig. 2. The incident wave height $H = 0.202$ m, period $T = 2.29$ s, and the wave direction is normal to the shoreline. The solution of Eq. (1) with the boundary conditions

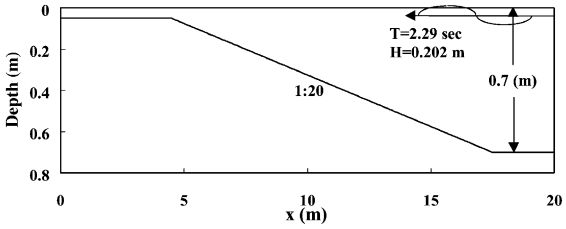

Fig. 2. Model problem beach with a uniform slope 1/20.

described in section 2 for $\gamma = 0$ is shown in Fig. 3, indicating an increase in wave height in the shoreward direction due to shoaling. The hydraulic model data, on the other hand, show a general decrease in the shoaling area due to breaking effects. The salient features of the various parameterizations used to describe γ and their implementation are described below.

4.1. Battjes and Janssen (1978) criterion (BJ)

$$\gamma = \frac{\alpha}{\pi c_g}\omega Q_b \frac{1}{b^2} \tag{23}$$

where α is an adjustable constant (standard value = 1),

$$Q_b = \exp\left[-(1-Q_b)/b^2\right] \tag{24}$$

$$b = \frac{H}{\sqrt{2}\,H_m} \tag{25}$$

In Eq. (25), H is the local wave height and H_m is the maximum allowable wave height defined by Miche's criterion with the wave breaking parameter γ_0 as

$$H_m = \frac{0.88}{k}\tanh\left[\frac{\gamma_0}{0.88}kd\right] \tag{26}$$

In shallow water, Eq. (26) can be simplified as $H_m = \gamma_0 d$ (where d is the local water depth and γ_0 has a standard value of 0.8). On the other hand, the breaking factor γ in Eq. (24) tends to 0 (no breaking occurs) for $Q_b \to 0$. Q_b is almost 0 ($Q_b = 1.5 \times 10^{-5}$) for $b = 0.3$ in Eq. (24). A lower limit for wave breaking may then be obtained from Eq. (25):

$$H_b = 0.3\sqrt{2}\,H_m \tag{27}$$

If the wave height $H \le H_b$, the value of γ would be 0 (non-breaking); otherwise, γ is estimated by using Eq. (23).

Although the problem is one-dimensional, solutions were obtained on a two-dimensional grid to ensure that the interfacing of the two one-dimensional sections and the semicircular open boundary was appropriate. A semicircle and the coastline formed the boundaries of a two-dimensional finite-element grid containing 125,584 triangular elements. The fully absorbing coastline was placed at $x = 0$ at a depth of 0.05 m. Eq. (13) converged after eight nonlinear iterations (Fig. 4), and its solution was used to force the two-dimensional Eq. (1), which converged after 12 non-linear iterations. Completely one-dimensional solutions with no spurious effects were obtained. The results along a cross-shore transect are shown in Fig. 3; the agreement between model results and laboratory data is satisfactory.

Each round of the solution for a specified γ requires several thousand iterations and the overall process is highly time-intensive. An attempt was

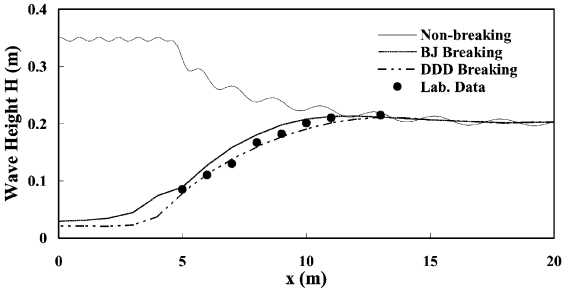

Fig. 3. Wave height comparison for uniform slope bathymetry, BJ and DDD criteria.

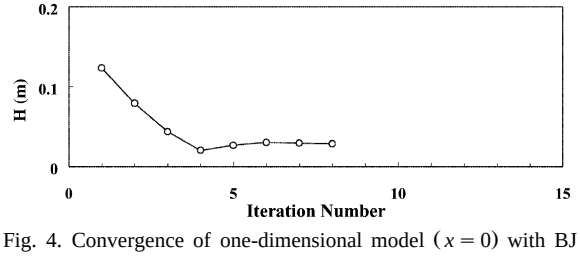

Fig. 4. Convergence of one-dimensional model ($x = 0$) with BJ criterion.

therefore made to combine the iterations for γ with the conjugate gradient iterations. γ was initially set equal to 0 and conjugate gradient iterations were performed until ε reached 10^{-10} for a linear solution. Thereafter, γ was updated every 100 iterations using the latest value of γ. This procedure did not converge uniformly, particularly when the effects of breaking were significant. This is further evidence that perturbations to the iterative techniques (for instance, by modification of γ or introduction of finite element equations with different boundary conditions) can impede the progress towards convergence observed by Oliveira and Anastasiou (1998) for their finite-difference model. This effort was therefore abandoned.

4.2. Dally et al. (1985) criterion (DDD)

$$\gamma = \frac{\chi}{d}\left[1 - \frac{\Gamma^2 d^2}{H^2}\right] \tag{28}$$

where H is the local wave height, d is the local depth, and Γ and χ are parameters known as the stable wave factor and wave decay factor. These two non-dimensional parameters (Table 1) were determined by Dally et al. (1985) for different beach slopes on the basis of the laboratory data of Horikawa and Kuo (1966). In this paper, Γ and χ were set to 0.4 and 0.11 for all test-cases.

The lower limit of wave breaking (i.e. $\gamma = 0$) may be obtained from Eq. (28) as follows:

$$H_b = \Gamma d \tag{29}$$

In the simulations, the value of γ is set to be 0 (non-breaking) if the wave height H estimated in the previous iteration is less than H_b, otherwise γ is estimated by using Eq. (28).

Table 1
Best fit values Γ and χ vs. bottom slope, after Dally et al. (1985)

Slope	Γ	χ
1/80	0.350	0.100
1/65	0.355	0.115
1/30	0.475	0.275

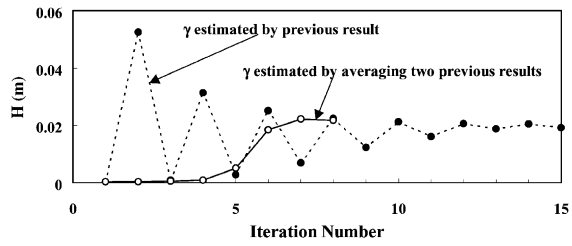

Fig. 5. Convergence of one-dimensional model ($x = 0$) with DDD criterion.

Unlike the simulations with the BJ criterion, the nonlinear iterations using the DDD criterion did not converge for the two-dimensional model to the specified tolerance after the maximum number of iterations. Investigation revealed perturbations (Fig. 5, dashed line) in the solution of Eq. (13) used to obtain the forcing functions for the two-dimensional model. After 15 iterations, the tolerance criterion was nearly met ($\delta = 1.21 \times 10^{-3}$) for Eq. (13), but the resulting two-dimensional solution was characterized by noise in the area where breaking is important. Detailed examination of the two-dimensional results showed that successive solutions at many nodes in shallow areas oscillated considerably between high and low no matter how many iterations were used. Such oscillations and occasional non-convergence were encountered in other formulations also. Due to the inter-connectedness of the grid points and the differences in the breaking formulations, it is difficult to pinpoint the exact cause of these oscillations (which did not occur with the BJ criterion), but it may be surmised that they stem from variations in γ as the iterations proceed. In shallow areas, the first round (with $\gamma = 0$) produced large wave heights, which lead to a high breaking factor and a subsequently damped solution for the second round. In the following round, the breaking factor is consequently negligible, leading to a solution similar to the non-breaking solution, and so on. To remedy this problem, γ was estimated on the basis of the average of two previous solutions. This technique did smooth the perturbations and accelerated convergence. The one-dimensional boundary forcing model converged in eight non-linear iterations with $\delta = 4.03 \times 10^{-4}$ (Fig. 5, solid line) and the two-dimensional model in 10 non-linear iterations with $\delta = 6.24 \times 10^{-4}$; the solu-

tions compare very well against laboratory data as shown in Fig. 3. The averaging technique was therefore used while implementing the DDD criterion in the verification described in Section 5.

4.3. Massel (1992) criterion (M)

$$\gamma = \left[\left(1 + 0.65\frac{H}{d}\right)\left(1 - 0.35\frac{H}{d}\right)\right]^{-1} \frac{\sigma H}{\pi c_g d} \qquad (30)$$

In this formulation, it is noted that, $\gamma < 0$ if $H > 2.85d$. An upper bound of $H_m = 2.85d$ was therefore placed on model estimates of wave height before estimating γ for the next round of iterations.

When the M criterion was used, both the one-dimensional forcing Eq. (13) and the two-dimensional model Eq. (1) converged in 10 iterations. As with the BJ criterion, averaging the previous two results to estimate γ led to smoother and accelerated convergence in six iterations (not shown). However, the solution (Fig. 6) agrees with data less favorably than with the BJ and DDD models. The breaking effect is excessive and appears to start further offshore than in Fig. 3. It was speculated that the underestimation was caused by the absence of a lower limit for wave breaking such as Eqs. (27) or (29), allowing the waves to experience breaking at all times (except when $H = 0$). A lower limit of $H_b = \eta d$ (comparable to the BJ and DDD criteria) was therefore introduced in the simulations with the M criterion (this combination is denoted by $M + H_b$ hereafter). This adjustment produced improved results (Fig. 6) when γ was estimated using the average of two previous results (when γ was estimated using only the previous result, the introduction of the lower limit impeded convergence, as in the case of the DDD criterion). Some tests were done to identify an appropriate value of η. The frequently used value of 0.78 produced the results shown in Fig. 6. The averaging technique with and without a lower limit was used for applications described in Section 5.

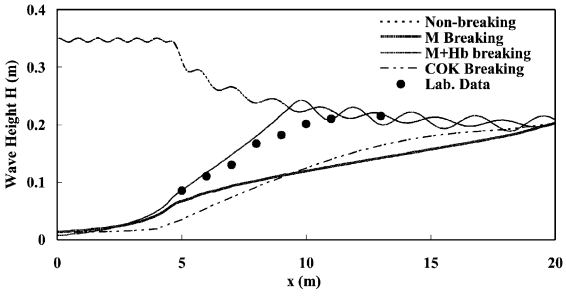

Fig. 6. Wave height comparison for uniform slope bathymetry, M and COK criteria.

4.4. Chawla et al. (1998) criterion (COK)

For inclusion in their parabolic approximation model based on Eq. (1), Chawla et al. (1998) adopted the statistical wave breaking formulation of Thornton and Guza (1983). Considering the monochromatic wave as an extreme condition of spectral wave, their breaking criterion may be written as:

$$\gamma = \frac{3\sqrt{\pi}}{2} \frac{\sigma B^3}{C_g \lambda^4 d^5} H^5 \qquad (31)$$

where the parameters B and λ were assigned values of 1.0 and 0.6, respectively, by Chawla et al. (1998). Using Eq. (31) in Eq. (1) led to oscillating solutions between iterates when γ was based on the previous iterate. However, estimation of γ based on the average of two previous solutions led to smooth convergence for both the one-dimensional Eq. (13) and the two-dimensional Eq. (1). The solution, though, shows a considerable underestimation relative to the data (Fig. 6), as with the M criterion. Introduction of a lower limit (such as setting $\gamma = 0$ for wave heights smaller than an appropriately defined H_b) did not improve results in this case; in fact the solutions diverged. The averaging technique with no lower limit was therefore used in Section 5.

4.5. Isobe (1999) criterion (I)

Isobe (1999) gave a parameterization for γ that depends on the bottom slope, and the relative depth $\lambda\ (= H/d)$; in this formulation, γ is zero when λ is less than a predetermined parameter λ_b, which depends on the deep-water wavelength, the local depth, and the bottom slope. When this breaking model was used with Eq. (1), we were unable to obtain convergence, regardless of the manner in which γ was estimated (i.e. based on the previous result or on the

average of two previous results). Results of the one-dimensional model oscillated considerably and did not converge even after 50 iterations. Obviously, this oscillating forcing function cannot produce stability in the two-dimensional model. Further, the definition of the bottom slope at all grid points in an arbitrarily varying domain with waves propagating in many directions is difficult (also noted by Booij et al., 1999). In view of these difficulties, the I-criterion is not further investigated in this paper (although other modelling approaches do utilize this formulation, e.g. Isobe, 1999).

5. Verification and practical application

To verify model performance in more complex applications, further simulations were made with the two-dimensional numerical model. The tests consist of wave propagation over a bar-trough bathymetry, over a transect in the North Sea with arbitrarily varying depths, around breakwaters on a sloping beach, and in Ponce de Leon Inlet in Florida. In all cases, hydraulic model or field data are available for model verification. In the first two cases, the bathymetry varies only in the offshore direction, i.e. they are essentially one-dimensional problems. However, simulations are performed with the two-dimensional model. The other three problems contain bathymetric or other variations in both x and y directions (in the event of occasional slow convergence the result after 15 non-linear iterations is shown).

Experimental data for wave shoaling, reflection, and breaking over the bar-trough bottom were obtained by Battjes and Janssen (1978). In view of the overall similarity of the parameters for this test to those of the linear slope case described earlier, we do not display the results of our simulation. We merely note that deviations from a linear slope create a marked undulating effect in the data (compared with data for the linearly sloping beach). The BJ and DDD model captured this feature very well. The COK and M models underestimated the data (as in the sloping beach case); see summary of results in Table 2. Instead, we show results for the North Sea test, since the transect along which field data were collected (Oelerich and Dette, 1988) and the relevant wave parameters (Fig. 7a) represent, coincidentally, an approximately scaled-up version of the linear slope and bar-trough bathymetry tests of Battjes and Janssen (1978). Results shown in Fig. 7b and Table 2 again suggest that the BJ, DDD, and the M + H_b models provide the best match with field data. As a consequence of the consistent underestimation resulting from the M and COK parameterizations, the results of these two models are not shown hereafter; they are only summarized in Table 2.

Table 2
Summary of model performance, model vs. data, RMS errors (%)

Test	Breaking parameterization				
	BJ	DDD	COK	M	M + H_b
Uniform slope	0.08	0.04	0.41	0.33	0.44
Bar-trough bathymetry	0.07	0.11	0.42	0.42	0.17
North Sea	0.06	0.05	0.25	0.23	0.08
Shore perpendicular breakwater					
$x = 6.0$ m	0.19	0.20	0.21	0.17	0.21
$x = 5.0$ m	0.20	0.21	0.22	0.21	0.21
$x = 4.0$ m	0.10	0.14	0.24	0.21	0.13
Shore parallel breakwater					
$x = 6.2$ m	0.12	0.17	0.29	0.34	0.09
$x = 5.8$ m	0.12	0.12	0.16	0.46	0.11
$x = 4.0$ m	0.16	0.18	0.28	0.46	0.15
Ponce inlet					
Transect 1					
$T = 8.0$ s, $H_i = 0.95$ m	0.20	0.20			
$T = 10.0$ s, $H_i = 0.93$ m	0.21	0.20			
$T = 15.0$ s, $H_i = 0.78$ m	0.19	0.18			
Transect 2					
$T = 8.0$ s, $H_i = 0.95$ m	0.33	0.32			
$T = 10.0$ s, $H_i = 0.93$ m	0.33	0.30			
$T = 15.0$ s, $H_i = 0.78$ m	0.32	0.25			
Transect 1 (spectral waves)		0.11			
Transect 2 (spectral waves)		0.36			

In the case of breakwaters on sloping beaches, the hydraulic model data of Watanabe and Maruyama (1986) were used. Two cases are considered. In the first case, a detached breakwater is placed parallel to the shoreline on a plane beach with a uniform slope of 1/50 (Fig. 8a). The breakwater was designed to almost perfectly reflect the normally incident waves. A two-dimensional grid with 70,600 triangular elements was used, with a fully absorbing coastal boundary located at a depth of 0.0025 m. The breakwater was given a thickness of 0.06 m. Numerical

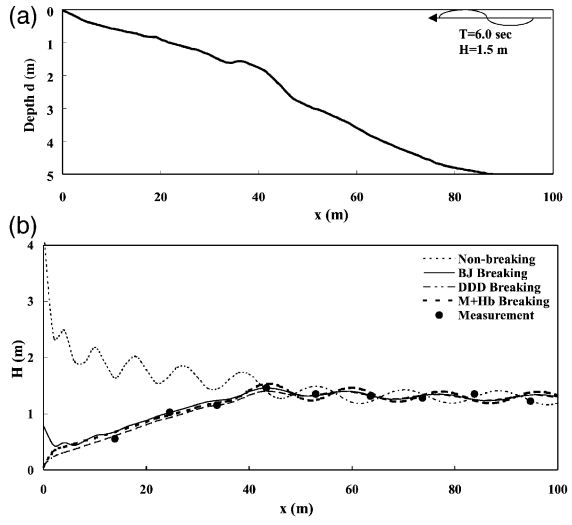

Fig. 7. (a) Depth profile, North Sea sta; after Oelerich and Dette (1988). (b) Cross-shore wave height comparison; data from Oelerich and Dette (1988).

solutions are compared with measured data in Fig. 8b for three cross-shore transects. While all five models captured the essential features of the data in a qualitative sense, the BJ and $M + H_b$ generally provided a better quantitative fit to the data than the others (Table 2).

In the second case, a jetty placed was perpendicular to the shoreline. The bathymetry and the incident wave conditions are the same as before, except that the incident wave angle is 60°. The modelled phase diagram, depicted in Fig. 9a, shows the expected bending of the waves as one goes from offshore to nearshore and no spurious oscillations that could be attributed to poor boundary conditions. This demonstrates the importance of interfacing the two-dimensional model with an appropriate model (viz. Eq. 13) for the exterior. Modelled wave heights are compared with the data of Watanabe and Maruyama (1986) in Fig. 9b for three cross-shore transects. In general, all models showed significant deviations from the non-breaking results, and the BJ, DDD, and $M + H_b$ models provide the best match with the data. Along $x = 4$ m, all results (including the non-breaking results) appear to underestimate the hydraulic model data for $y > 2$ m (i.e. before the onset of significant breaking). The reasons for this are not clear.

Finally, the model was applied to Ponce de Leon Inlet (Florida), of which detailed field and hydraulic model studies are being conducted by the US Army Corps of Engineers (Harkins et al., 1997). The geometry (Fig. 10) consists of an exposed coastline, an inlet leading to the Halifax and Indian Rivers, a jetty with a scoured area to its side, a large promontory with shoals and trenches that juts out toward the ocean next to the jetty, and a bathymetry that is generally sloping in the offshore direction. Simula-

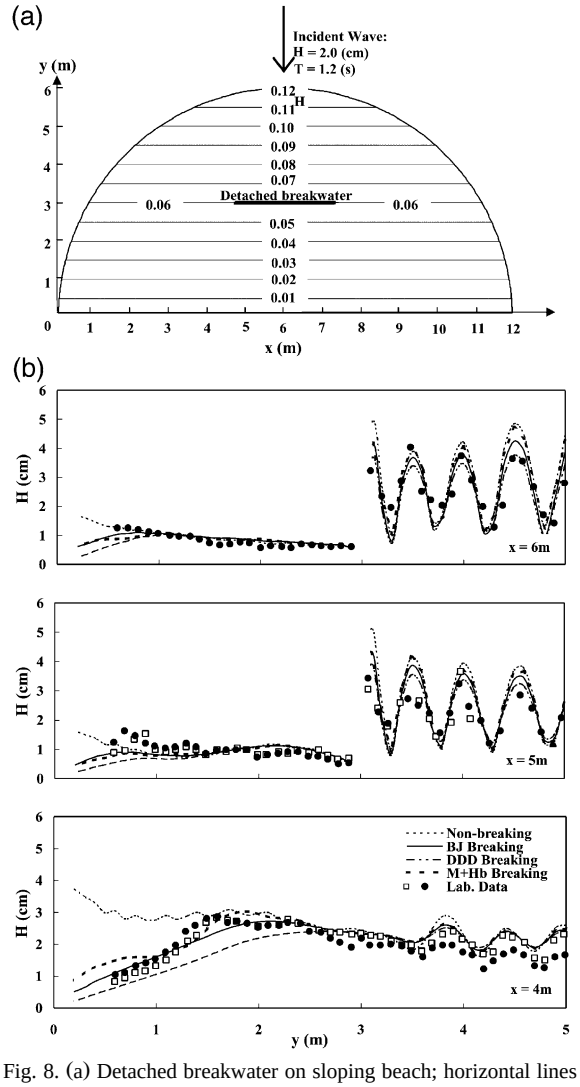

Fig. 8. (a) Detached breakwater on sloping beach; horizontal lines represent depth contours (m). (b) Wave height comparison for problem in (a) (note: breakwater is at $y = 3$ m).

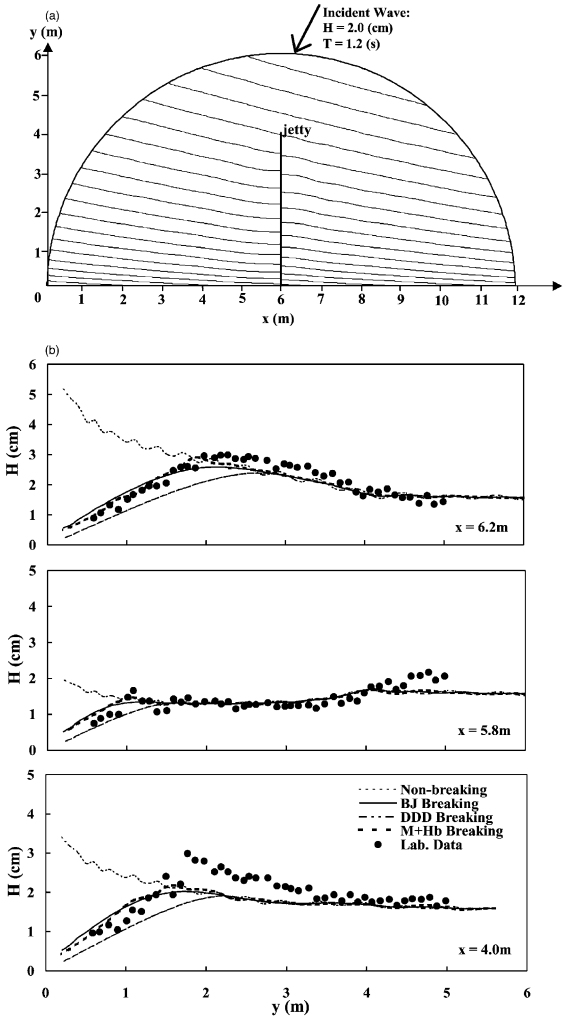

Fig. 9. (a) Jetty on sloping beach. Phase diagram, contour lines represent cosine of phase = 0. (b) Wave height comparison for problem in (a).

tions were performed on a wavelength-dependent grid containing 265,119 nodes and were found to be largely insensitive to the reflection coefficient assigned to the jetty. For this problem with an arbitrarily varying bathymetry, the effect of the boundary conditions proposed here may be seen in Fig. 11, where a comparison with the traditional method of using constant depths in the exterior is given (e.g. Xu et al., 1996 and models cited therein) for the case of a 15-s incident wave of height 0.78 m. The constant depth assumption induces artificial diffraction, indicated by breaks in the phase diagram (Fig. 11a, top) and large waves even in shallow areas near the open boundary (Fig. 11b, top). These spurious effects can often permeate the entire solution. With the new method, a more satisfactory solution is obtained (Fig. 11a and b, bottom).

Fig. 12 shows breaking and non-breaking results along transect 3 shown in Fig. 10; breaking clearly plays a significant role. In Figs. 13 and 14, hydraulic model data along the two of the transects shown in Fig. 10 are compared to numerical results for three normally-incident monochromatic wave conditions. The numerical results appear to exhibit a higher level of variability than the hydraulic model data (especially along Transect 2). However, it may be noted that the bathymetric variations in the vicinity of the transects are comparable to those in the shoal studies of Berkhoff et al. (1982) and Vincent and Briggs (1989), where data obtained at much greater resolution (approximately 5 data points per wavelength) indicate that wave height amplification factors vary from 0.2 to 2.6. It is possible, therefore, that the hydraulic model data for Ponce Inlet (obtained at a resolution of approximately 0.66 data points per wavelength) suffer from under-sampling. The numerical results show the same kind of variability as that observed in the shoal studies, suggesting that these results are reasonable. Further, the variability is less for the longer waves than for the shorter waves, which should be expected. The introduction of breaking tends to bring the model results closer to hydraulic model data in many locations. Table 2 provides a comparison of RMS errors for the numerical solutions (only the BJ and DDD models were used for the Ponce Inlet simulations in view of their

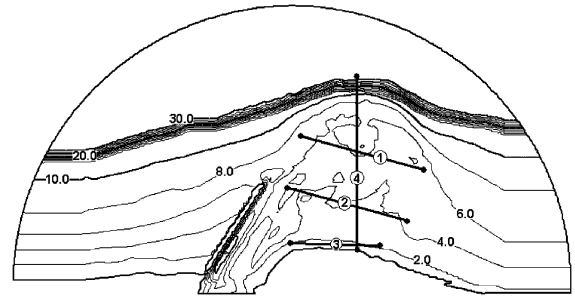

Fig. 10. Ponce de Leon Inlet, model bathymetry. Transects 1, 2, 3 and 4 used for wave height comparisons.

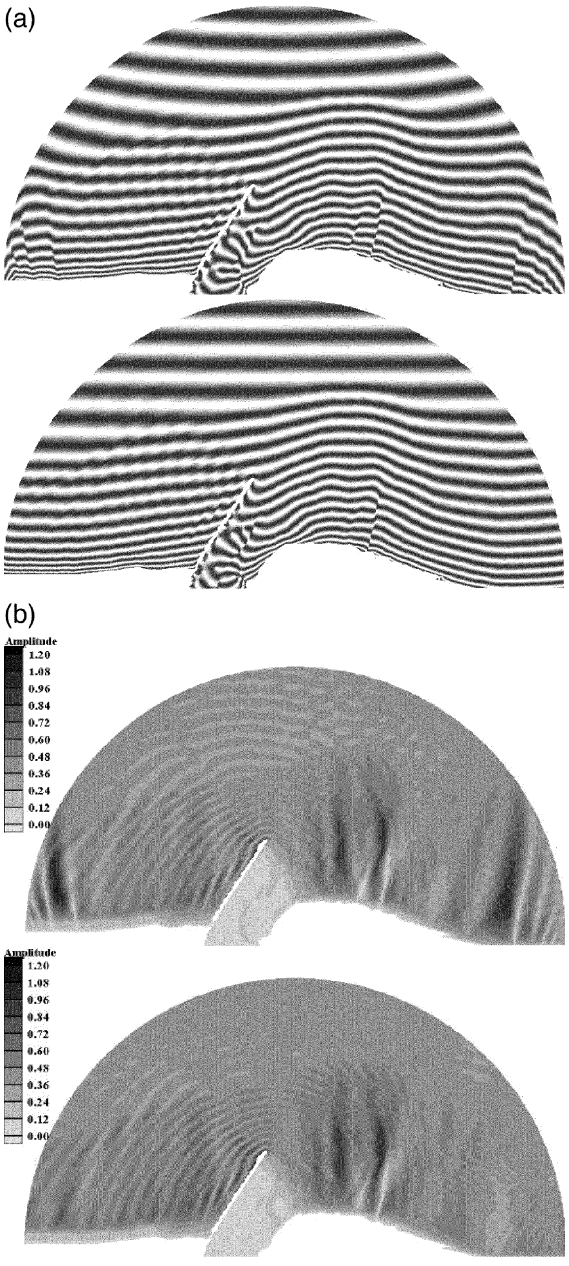

Fig. 11. (a) Ponce Inlet, modelled phase diagrams. Traditional method (top); present method (bottom). (b) Ponce Inlet, modelled wave heights. Traditional method (top); present method (bottom).

overall robustness observed in the previous tests). While the non-breaking and breaking results are fairly similar on the offshore Transect 1, both breaking models produce, in general, smaller errors along Transect 2.

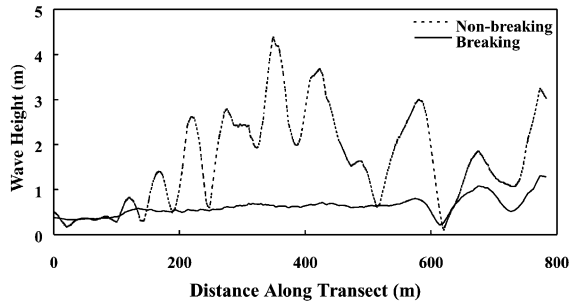

Fig. 12. Breaking and non-breaking results on Transect 3 for incident wave of $T = 10$ s, $H = 0.93$ m.

Simulations were also performed for an input TMA spectrum with a wrapped-normal directional distribution. The spectrum was decomposed into 66 monochromatic bins of size 0.13 Hz and 10°, and simulations were made for each monochromatic component. The results were subsequently assembled using linear superposition. The results (Fig. 15) exhibit far less variability for spectral conditions (as

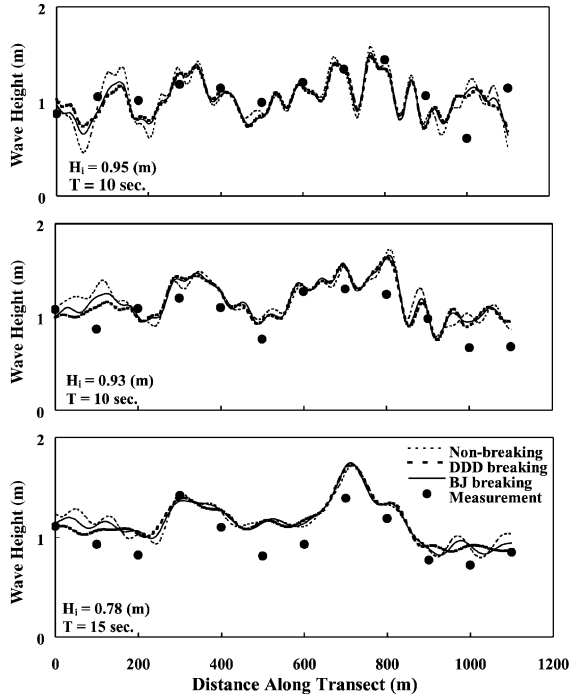

Fig. 13. Wave height comparison along Transect 1.

described in Panchang et al., 1990) and a generally good match with data, although some overestimation on Transect 2 persists (it is to be noted that these results involve no tuning of any kind for the coefficients associated with the breaking formulations). In view of this overestimation, an alternative strategy calculating the breaking factor on the basis of the significant wave height (SWH) instead of the component wave height was considered. This eliminates the independence of individual component simulations; the code was therefore modified so that one round of nonlinear iterations for all components was performed, the significant wave height calculated at each grid point, and this larger wave height used to estimate the breaking factor (Chawla et al., 1998). This approach is comparable to that used in the model SWAN (Booij et al., 1999) which has been extensively verified for areas with severe breaking. It led to much smaller wave heights, and as seen in Fig. 15 for Transect 4, led to the initiation of breaking occurring further offshore ($x = 1200$ m as opposed to $x = 1500$ m). While some improvement is seen along Transect 2, the availability of data in the nearshore areas (in the vicinity of Transect 3) would have permitted a more detailed quantitative validation of overall model performance.

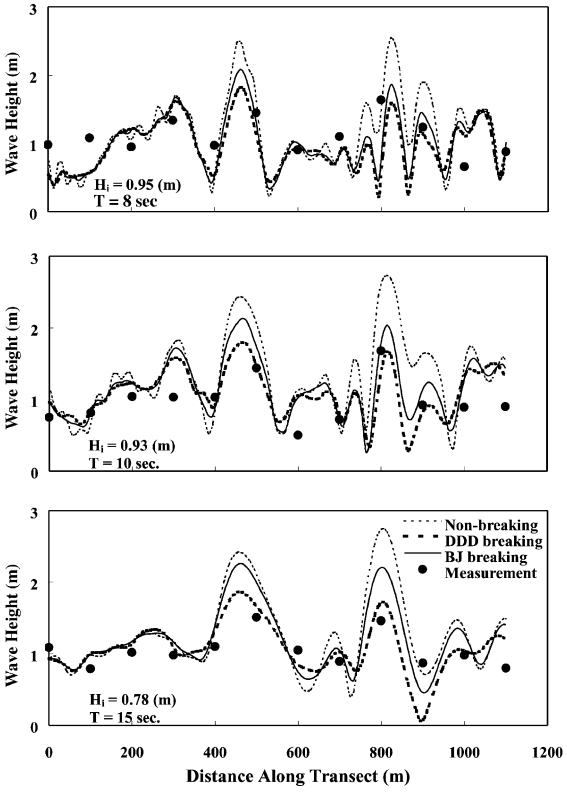

Fig. 14. Wave height comparison along Transect 2.

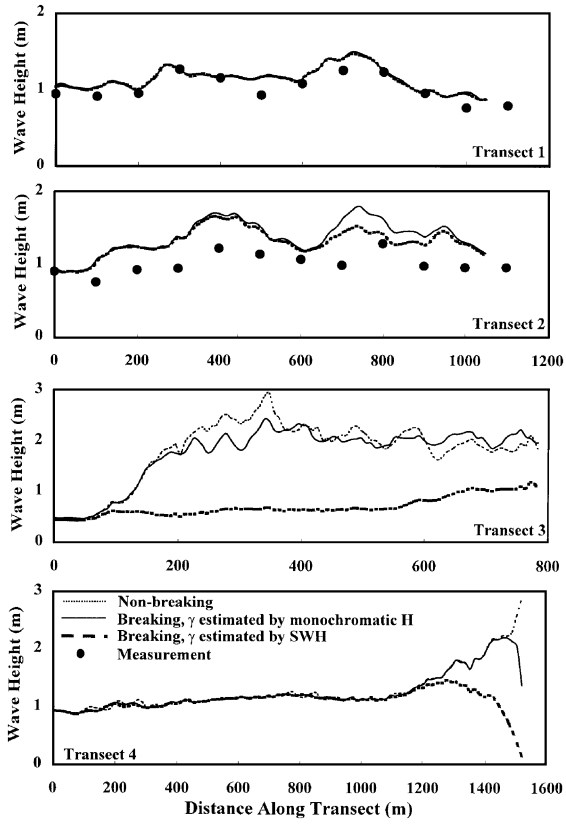

Fig. 15. Wave height comparison, for spectral wave input.

6. Summary and concluding remarks

The effect of wave breaking in most elliptic harbor wave prediction models is either completely absent or inadequately represented by traditional boundary conditions used to force the models. A strategy is designed to include breaking in a two-dimensional finite-element harbor wave model. It is based on an interfacing of Eqs. (1) and (13). Eq. (13) is first used to describe wave propagation, including breaking, in the exterior region, which is assumed to vary largely in the cross-shore direction along two

transects. Its solution is used as part of the forcing function for the two-dimensional Eq. (1) that is solved in the model domain. Nonlinear iterative strategies were developed for incorporating the breaking parameter γ.

The model was used with five breaking formulations. The I-criterion was found to be unsuitable within the context of the modelling scheme described here. In general, the absence of a lower breaking limit contributed to excessive dissipation (compared with data) in the COK and M formulations while the BJ, DDD, and $M + H_b$ formulations gave more accurate results, as seen in Table 2. Applications to real-world situations like the North Sea and Ponce de Leon Inlet tests demonstrate that the effects of breaking are indeed significant and that the model described here provides reasonable simulations for both monochromatic and spectral cases. The other formulations provided good results compared with data for the six applications considered in this paper. In nearly all cases considered, wave heights in the nearshore areas obtained from data as well as from the one-dimensional Eq. (13) were smaller than the non-breaking results. This justifies the inclusion of wave breaking not only in the computational model but also in the boundary conditions. If traditional boundary conditions based on non-breaking waves are used to force Eq. (1), a mismatch along the open boundary results, and consequently, spurious effects would propagate into the model domain.

Acknowledgements

Partial support for this work was received from the Office of Naval Research, the Maine Sea Grant Program, and the National Sea Grant Office. Assistance rendered by Karl Schlenker is gratefully acknowledged.

References

Battjes, J.A., Janssen, J., 1978. Energy loss and set-up due to breaking of random waves. Proc. 16th Int. Conf. Coastal Engg. ASCE, New York, pp. 569–587.

Behrendt, L., 1985. A Finite Element Model for Water Wave Diffraction including Boundary Absorption and Bottom Friction. Institute of Hydrodynamics and Hydraulic Engineering. Technical University of Denmark. Series Paper 37, 1985.

Berkhoff, J.C.W., Booy, N., Radder, A.C., 1982. Verification of numerical wave propagation models for simple harmonic linear water waves. Coastal Eng. 6, 255–279.

Booij, N., 1981. Gravity Waves on Water with Non-uniform Depth and Current. Doctoral thesis, Technical University of Delft, The Netherlands.

Booij, N., Ris, R.C., Hothuijsen, L.H., 1999. A third-generation wave model for coastal regions: 1. Model description and validation. J. Geophys. Res. 104 (c4), 7649–7666.

Bova, S.W., Breshears, C.P., Cuicchi, C., Demirbilek, Z., Gabb, H.A., 2000. Dual-level parallel analysis of harbor wave response using MPI and OpenMPI. Int. J. High Perform. Comput. Appl. 14 (1), 49–64.

Chawla, A., Ozkan-Haller, H.T., Kirby, J.T., 1998. Spectral model for wave transformation and breaking over irregular bathymetry. J. Waterway, Port, Coastal Ocean Eng. 124, 189–198.

Chen, H.S., 1986. Effects of bottom friction and boundary absorption on water wave scattering. Appl. Ocean Res. 8 (2), 99–104.

Chen, H.S., Houston, J.R., 1987. Calculation of water level oscillations in harbors. Instructional Rept., CERC-87-2, Waterways Expt. Stn., Vicksburg, MS.

De Girolamo, P., Kostense, J.K., Dingemans, M.W., 1988. Inclusion of wave breaking in a mild-slope model. In: Schrefler, Zienkiewicz (Eds.), Computer Modeling in Ocean Engineering. Balkema, Rotterdam, pp. 221–229.

Dally, W.R., Dean, R.G., Dalrymple, R.A., 1985. Wave height variation across beaches of arbitrary profile. J. Geophys. Res. 90 (c6), 11917–11927.

Demirbilek, Z., Panchang, V.G., 1998. CGWAVE: A Coastal Surface Water Wave Model of the Mild Slope Equation, Tech Rept CHL-98-26, US Army Corps of Engineers Waterways Expt Stn, Vicksburg, MS 39180.

Ebersole, B.A., 1985. Refraction–diffraction model for linear water wave. J. Waterway, Port, Coastal Ocean Eng. 111 (6), 939–953.

Foster, I., 1997. Designing and Building Parallel Programs. Addison-Wesley, Reading, MA.

Harkins, G.S., Puckette, P., Dorrell, C., 1997. Physical Model Studies of Ponce DeLeon Inlet, Florida. Tech Rept CHL-97-23, US Army Corps of Engineers Waterways Expt Stn, Vicksburg, MS 39180.

Horikawa, K., Kuo, C.T., 1966. A study on wave transformation inside surf zone. Proc. 10th Internat. Conf. Coastal Engg. ASCE, New York.

Isaacson, M., Qu, S., 1990. Waves in a harbour with partially reflecting boundaries. Coastal Eng. 14, 193–214.

Isobe, M., 1999. Equation for numerical modeling of wave transformation in shallow water. In: Herbich, J.B. (Ed.), Developments in Offshore Engineering. Gulf Publishing, Houston, pp. 101–162, Chap. 3.

Kamphuis, J.W., 1994. Wave height from deep water through breaking zone. J. Waterway, Port, Coastal Ocean Eng. 120 (4), 347–367.

Kostense, J.K., Meijer, K.L., Dingemans, M.W., Mynett, A.E., van den Bosch, P., 1986. Wave energy dissipation in arbitrar-

ily shaped harbours of variable depth. Proc. 20th Int. Conf. Coastal, 2002–2016.

Larson, M., 1995. Model for decay of random waves in surf zone. J. Waterway, Port, Coastal Ocean Eng. 121 (1), 1–12.

Li, B., 1994. A generalized conjugate gradient model for the mild slope equation. Coastal Eng. 23, 215–225.

Massel, S.R., 1992. Inclusion of wave-breaking mechanism in a modified mild-slope model. In: Banner, M.L., Grimshaw, R.H.J. (Eds.), Breaking Waves IUTAM Symposium, Sydney/Australia 1991. Springer-Verlag, Berlin, pp. 319–324.

Mattioli, F., 1996. Dynamic response of the lido channel to wave motion in the presence of movable barriers. Il Nuovo Cimento 19c (1), 177–194.

Mei, C.C., 1983. The Applied Dynamics of Ocean Surface Waves. Wiley, New York.

OARB, 1997. OpenMP Fortran Application Program Interface. OpenMP Architecture Review Board (OARB) v1.0, http://www.openmp.org, October 1997.

Oelerich, J., Dette, H.H., 1988. About the energy dissipation over bared beaches. Proc. 21th Int. Conf. Coastal Eng. 293–306.

Oliveira, F.S.B.F., Anastasiou, K., 1998. An efficient computational model for water wave propagation in coastal regions. Appl. Ocean Res. 20, 263–271.

Panchang, V.G., Ge, W., Pearce, B.R., Briggs, M.J., 1990. Numerical simulation of irregular wave propagation over a shoal. J. Waterway, Port, Coastal Ocean Eng. 116 (3), 324–340.

Panchang, V.G., Ge, W., Cushman-Roisin, B., Pearce, B.R., 1991. Solution to the mild-slope wave problem by iteration. Appl. Ocean Res. 13 (4), 187–199.

Panchang, V.G., Xu, B., Demirbilek, Z., 1999. Wave prediction models for coastal engineering applications. In: Herbich, J.B. (Ed.), Developments in Offshore Engineering. Gulf Publishing, Houston, pp. 163–194, Chap. 4.

Panchang, V.G., Chen, W., Xu, B., Schlenker, K., Demirbilek, Z., Okihiro, M., 2000. Effects of exterior bathymetry in elliptic harbor wave models. J. Waterway, Port, Coastal Ocean Eng. 126 (2), 71–78.

Schaffer, H.A., Jonsson, I.G., 1992. Edge waves revisited. Coastal Eng. 16, 349–368.

Thornton, E.B., Guza, R.T., 1983. Transformations of wave height distribution. J. Geophys. Res. 88, 5925–5938.

Tsay, T.-K., Liu, P.L.-F., 1983. A finite element model for wave refraction and diffraction. Appl. Ocean Res. 5 (1), 30–37.

Vincent, C.L., Briggs, M.J., 1989. Refraction–diffraction of irregular waves over a mound. J. Waterway, Port, Coastal Ocean Eng. 115 (2), 269–284.

Watanabe, A., Maruyama, K., 1986. Numerical modeling of nearshore wave field under combined refraction, diffraction and breaking. Coastal Eng. Jpn. 29, 19–39.

Xu, B., Panchang, V.G., Demirbilek, Z., 1996. Exterior reflections in elliptic harbor wave models. J. Waterway, Port, Coastal Ocean Eng. 122 (3), 118–126.

Zundell, A.K., Fugal, A.L., Jones, N.L., Demirbilek, Z., 1998. Automatic definition of two-dimensional coastal finite element domains. In: Babovic, V., Larsen, L.C. (Eds.), Hydroinformatics98, Proc. 3rd Internat. Conf. Hydroinformatics. A.A. Balkema, Rotterdam, pp. 693–700.